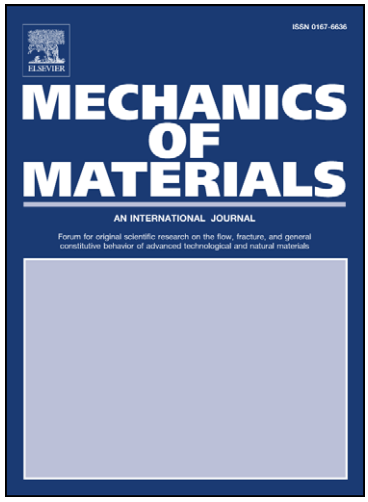

A Constitutive Model for Finite Deformation Response of Layered Polyurethane-Montmorillonite Nanocomposites

Amit K. Kaushik, Anthony M. Waas, Ellen M. Arruda

PII: S0167-6636(11)00022-6
DOI: 10.1016/j.mechmat.2011.01.005
Reference: MECMAT 1849

To appear in: *Mechanics of Materials*

Received Date: 6 April 2010
Accepted Date: 24 January 2011

Please cite this article as: Kaushik, A.K., Waas, A.M., Arruda, E.M., A Constitutive Model for Finite Deformation Response of Layered Polyurethane-Montmorillonite Nanocomposites, *Mechanics of Materials* (2011), doi: 10.1016/j.mechmat.2011.01.005

A Constitutive Model for Finite Deformation Response of Layered Polyurethane-Montmorillonite Nanocomposites

Amit K. Kaushik[a,b], Anthony M. Waas[c], Ellen M. Arruda[d,*]

[a] *Department of Mechanical Engineering, University of Michigan, Ann Arbor, MI 48109*
[b] *Current Address: Corporate Engineering Technologies Laboratory, The Procter and Gamble Company, 8256 Union Centre Blvd, West Chester, OH 45069*
[c] *Departments of Aerospace and Mechanical Engineering, University of Michigan, Ann Arbor, MI 48109*
[d] *Departments of Mechanical and Biomedical Engineering, Program in Macromolecular Science and Engineering, University of Michigan, Ann Arbor, MI 48109*

Abstract

A constitutive model is developed to predict the finite deformation response of multilayered polyurethane (PU)-montmorillonite (MTM) nanocomposites. In PU-MTM nanocomposites, the PU matrix in the vicinity of the MTM nanoparticles is modified leading to an interphase region, and its effect on the finite deformation response of these nanocomposites is largely neglected in many existing models. In this work, the entire spatial volume is considered to be occupied by multi-layers of bulk PU and effective particles which consist of MTM nanoparticles and the modified PU interphase region. A Langevin chain based eight chain model is used to capture the large stretch hyperelastic behavior of bulk PU. The effective particle component of the model consists of a linear elastic spring to capture the initial elas-

*Corresponding author
Email address: arruda@umich.edu (Ellen M. Arruda)
URL: http://www.umich.edu/~arruda (Ellen M. Arruda)

tic response, a non-linear viscoplastic dash-pot for the strain-rate dependent yield strength of nanocomposites, and a non-linear spring element in parallel to the dash-pot for the strain-hardening response. The model adopts the concept of amplified strain of the confined PU chains to accommodate the applied strain owing to the limited strain in the MTM nanoparticles. The constitutive model predicts all the major features of the stress-strain constitutive response of a family of PU-MTM nanocomposites including the initial linear elastic response, yield strength and post yield strain hardening for all volume fractions of MTM nanoparticles, thus confirming the efficacy of the proposed constitutive model.

Keywords: polymer nanocomposites, constitutive model, interphase, finite deformation, montmorillonite, amplified stretch

1. Introduction

Efforts to model the enhancements in mechanical properties of polymers that result from incorporation of rigid inclusions date back to early 1940s. Smallwood (Smallwood, 1944), in 1944, predicted the small strain Young's modulus of particle-filled solids. In the following year, Guth (Guth, 1945) theoretically estimated the stiffness of a rubber-carbon black system. These estimates were based on Einstein's work determining the viscosity of colloidal suspensions and emulsions (Einstein, 1906). Both estimates determined the stiffness of the system to be a non-linear function of the volume fraction of the filler particles and were accurate at low volume fractions. Since then, several models have been proposed to predict the enhancement in mechanical properties of composites with a few of them being variations of these

estimates (Vand, 1996; Mooney, 1951; Budiansky, 1965; Halpin, 1969; Mori and Tanaka, 1973; Govindjee, 1997; Luo and Daniel, 2003; Sheng et al., 2004; Odegard et al., 2005; Anthoulis and Kontou, 2008). Many of these approaches have been found to provide robust predictions in the case of polymer nanocomposites. However, they have been employed to model only the elastic properties of nanocomposites with Halpin-Tsai (Halpin, 1969) and Mori-Tanaka (Mori and Tanaka, 1973) models among the most widely accepted. Anthoulis and Kontou (Anthoulis and Kontou, 2008), however, have recently presented a model to formulate the elastoplastic response of epoxy-clay nanocomposites based on Mori-Tanaka theory (Mori and Tanaka, 1973) for the elastic stiffness and the Budiansky and Wu model (Budiansky and Wu, 1962) for the plastic response. More recently, there have been developments in the constitutive modeling of toughened semi-crystalline polymer systems to describe their finite deformation response at a range of strain rates and sample temperature (Zaïri et al., 2010b,a).

For the case of nanocomposites, computational chemistry approaches, including molecular dynamics (MD) simulations, have been utilized to investigate several structural and dynamic details at the atomic scale, e.g., changes in polymer mechanics in proximity to nanoparticles (Smith et al., 2003) leading to an interphase and effects of filler sizes on mechanical properties of polymer nanocomposites (Adnan et al., 2007). In general, role of the interphase is vital in the enhancement of mechanical properties of nanocomposites as opposed to conventional composites. In nanocomposites, the surface area to volume ratio of nanoinclusions is several orders of magnitude higher than that of conventional fillers in composites. Thus, the interphase contributes sig-

nificantly to the overall properties of the nanocomposite. Although research groups have investigated the properties of interphases using computational approaches, experimental determination of properties and morphologies of the interphase is a challenging task. MD simulations, for example, have been used to determine the properties and size of the interphase with certain assumptions (Boutaleb et al., 2009). These simulations yield the properties of polymer molecules in a time period of a few femtoseconds up to a few nanoseconds, several orders of magnitude in time lower than that required in the continuum-based calculations.

Many existing models for composites partition the total volume into particle and matrix domains. However, these can not be applied to nanocomposites due to the nanometer length scale morphology of nano-fillers and the modified matrix in proximity to these nanofillers leading to the interphase region (Vaia et al., 1997; Brune and Bicerano, 2002; Ramanathan et al., 2005; Kaushik et al., 2009). Considering this, several recent works have explicitly or implicity used the idea of pseudoparticle or effective particle (Luo and Daniel, 2003; Sheng et al., 2004; Fisher et al., 2003). For instance, Sheng et al. (Sheng et al., 2004) represented multiple sheets of intercalated clay and the inter-layer galleries as an effective particle. This was used in order to account for the potentially low shear modulus of inter-layer galleries. In the present paper, we have also utilized the idea of effective particle to present the continuum-based model predictions of the finite deformation response of multi-layered polyurethane (PU)- montmorillonite (MTM) nanocomposites with a broad range of volume fractions of MTM nanoparticles. Here, we model the nanocomposite as a heterogenous material consisting of two

phases: bulk PU and an effective particle. The effective particle is defined and employed to represent the stratified layer of MTM nanoparticles and the interphase region (Kaushik et al., 2009). The overall mechanical properties of nanocomposites in terms of elastic stiffness, yield strength and strain hardening are predicted via a combination of constitutive models of Boyce, Parks and Argon (Boyce et al., 1988) and Arruda and Boyce (Arruda and Boyce, 1993b). A notion of amplified strain in the interphase region is adopted to accommodate the applied strain owing to the limited strain in MTM nanoparticles (Mullins and Tobin, 1965). The model is then validated against the major features of uniaxial stress-strain constitutive responses in tension including linear elastic response, yield strength and post yield strain hardening for all the volume fractions of MTM nanoparticles.

2. Experimental Details

The finite deformation true stress vs. true strain response of PU and PU-MTM nanocomposites in tension with a wide range of volume fractions of MTM nanoparticles at a strain rate, $\dot{\epsilon} = 0.005$/sec is shown in Figure 1. Experiments characterizing the materials, their structural, mechanical and thermal properties are described in detail in (Kaushik et al., 2009). Briefly, PU consisted of a large amount of soft segments in a rubbery-like state imparting a low, mildly pronounced average yield point and modulus of 2 MPa and 25 MPa respectively; and a large average nominal strain-to-failure of 4.1 (average true strain-to-failure of 1.63). A series of multilayered PU-MTM nanocomposites was manufactured, with alternating PU and MTM nanolayers, using a layer-by-layer manufacturing technique (Decher, 1997; Podsiadlo

et al., 2007; Kotov, 2001). The systematic variation in MTM nanoparticle volume fraction was achieved by varying the thickness of the PU nanolayer and therefore the MTM layer separation. The PU-MTM nanocomposites deformed with an enhanced and much more pronounced yield strength and modulus, which increased with an increase in MTM nanoparticle volume fraction. The nanocomposites deformed plastically resulting in an increased residual strain on unloading with an increase in the volume fraction of MTM nanoparticles (Kaushik, 2010). The thickness of the PU layer (or the MTM layer separation) was found to control the finite deformation response of PU-MTM nanocomposites (Table 1) (Kaushik et al., 2009). The presence of alternate MTM nano-layers modified the bulk PU matrix in close proximity to the nanoparticles resulting in an interphase region consisting of confined and stiffened PU chains with restricted mobility. All of the bulk PU chains were modified to these confined and stiffened PU chains at ~ 12 v.% MTM nanoparticles resulting in a transition from ductile to brittle deformation response. The modification of bulk PU chains in the interphase region is believed to be the reason for pronounced yield phenomena and plastic deformation in the PU-MTM nanocomposites. The enhancement in the yield strength is due to the increased resistance to plastic deformation of these reduced mobility PU chains.

In this work, we have conducted tests on the PU-MTM5 nanocomposite (with 5 v.% MTM nanoparticles) at $\dot{\epsilon} = 0.01/\text{s}$ and $0.05/\text{s}$ using the tensile tester described in (Kaushik et al., 2009) and (Larkin et al., 2006). The PU-MTM5 nanocomposite dog bone specimens were loaded at room temperature ($\sim 23\,^{\circ}\text{C}$) and $\sim 30\%$ humidity until failure. The gage section of the

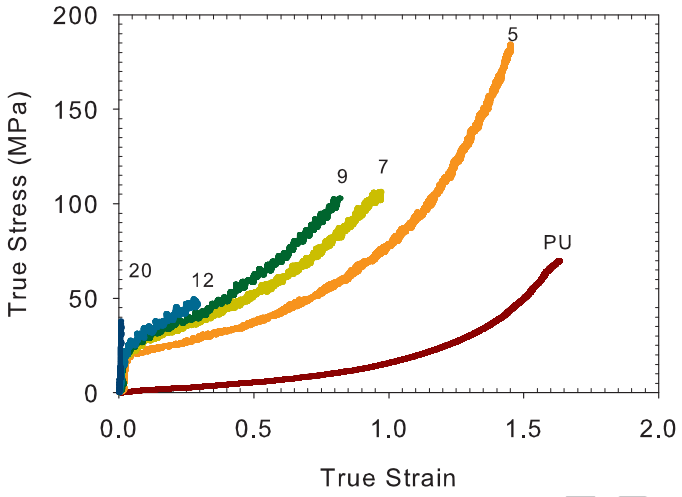

Figure 1: Representative true stress-strain constitutive response of PU-MTM nanocomposites at a strain rate of 0.005/s, humidity of $\sim$ 30%, and room temperature ($\sim$ 23 °C) (Kaushik et al., 2009). Numbers indicate average volume fractions of MTM nanoparticles.

specimens deformed uniformly macroscopically with no predominant necking phenomenon. The nominal stress (force/cross-section area) and nominal strain (measured using digital image correlation) were converted to true stress and true strain by assuming incompressibility (Kaushik et al., 2009).

3. Modeling Approach

A schematic of a nano-structure that both approximates the actual nanocomposite structure and facilitates the mechanical modeling is shown in Figure 2. Here, the total spatial volume is considered to be occupied by multi-layers of bulk PU matrix and effective particles. The thickness of bulk PU ma-

sample name	MTM loading v_p (v. %)	film thickness (μm)	avg. bilayer thickness, t_b (nm)	modulus (GPa)	yield strength (MPa)
PU	0	− − −	− − −	0.025±0.005	2.0±0.1
PU-MTM5	5	16.1±1.2	53	0.45±0.05	21.1±0.3
PU-MTM7	7	8.7±0.7	31	0.74±0.10	25.2±0.4
PU-MTM9	9	6.8±0.7	24	1.0±0.2	27.3±0.4
PU-MTM12	12	5.1±0.3	17	1.65±0.15	28.5±0.7
PU-MTM20	20	3.2±0.1	11	3.6±0.2	− − −

Table 1: Summary of structural and mechanical properties of PU and PU-MTM nanocomposites (Kaushik et al., 2009)

trix is taken as t_{PU}. The effective particle is composed of stratified layers of MTM nanoparticles and the interphase region consisting of confined and stiffened PU chains. The stratified layer of MTM nanoparticles of thickness t_{strat} is composed of approximately three layers of MTM nanoparticles each 1 nm thick (Kaushik et al., 2009). The thickness of the interphase on either side of the MTM stratified layer is t. The effective particle is employed as a basic element in the constitutive model to assess the influence of the MTM nanoparticles on the overall nanocomposite constitutive response. The volume fraction of effective particle, v_{ep} is determined as (c.f. Figure 2 (B)):

$$v_{ep} = \frac{t_{estrat} + 2t}{t_b} \tag{1}$$

i.e.

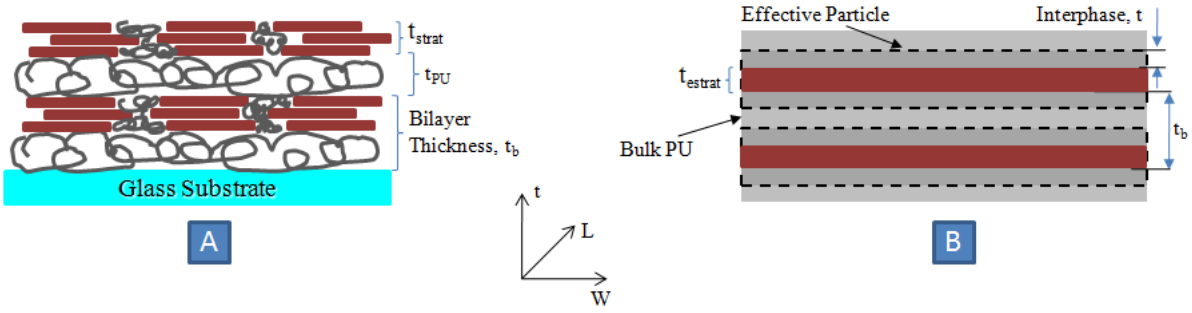

Figure 2: (A) A schematic of nanostructure of the PU-MTM nanocomposite (Kaushik et al., 2009). (B) An equivalent representative volume element of the PU-MTM nanocomposite illustrating the interphase and effective particle concepts.

$$v_{ep} = v_p + \frac{2t}{t_b} \tag{2}$$

where t_{estrat} is a thickness equivalent to t_{strat} in Figure 2 (A), v_p is the volume fraction of MTM nanoparticles and t_b is the average bilayer thickness (Table 1). As evident from Equation 2, v_{ep} increases with an increase in t. In our modeling approach, we set t as a free fitting parameter and determine its value based on the convergence of the fitting procedure. v_{ep} also depends on both v_p and t and from Table 1 it is clear that t_b is itself dependent upon the particle volume fraction.

3.1. Modeling Constituents

In the current work, interest is in modeling the true stress-strain behavior of PU and PU-MTM nanocomposites. A constitutive model for capturing the stress-strain behavior of PU has been developed by Qi and Boyce (Qi and Boyce, 2005). Their model decomposed the material behavior into a

rate-independent equilibrium part representing the soft segments and a rate-dependent viscoelastic-plastic part representing the hard segments of PU. As the volume fraction of hard segments decreases to zero, this model reduces to the Langevin chain based eight-chain model (Arruda and Boyce, 1993b).

The proposed three-dimensional constitutive model is decomposed into components representing the bulk PU and effective particle (Figure 3). The bulk PU used in the current nanocomposites has a significantly low volume fraction of hard segments (Kaushik et al., 2009; Ke and Stroeve, 2010). For modeling purposes we assume that the PU is composed of soft elastomeric segments only. Hence, we model the bulk PU with a non-linear hyperelastic rubbery spring element capturing the entropy change due to molecular orientation of PU chains. The component representing the effective particle comprises three elements: a linear spring to characterize the initial elastic response; a non-linear spring accounting for an anisotropic resistance to molecular chain orientation; and a visco-plastic dashpot accounting for the rate and temperature-dependent yield monitoring an isotropic resistance to chain segment rotation. We note from the representative volume element that the effective particle and bulk PU experience the same deformation (deformation direction is along W, c.f. Figure 2). Hence, the constitutive elements representing the effective particle are modeled "in parallel" to the hyperelastic rubbery spring element representing bulk PU (Figure 3).

The kinematics of three-dimensional finite strain deformation is presented here briefly. Readers are advised to refer (Boyce et al., 1988) and (Arruda and Boyce, 1993b) for more details. Owing to the configuration of the constitutive elements (ref. Figure 3),

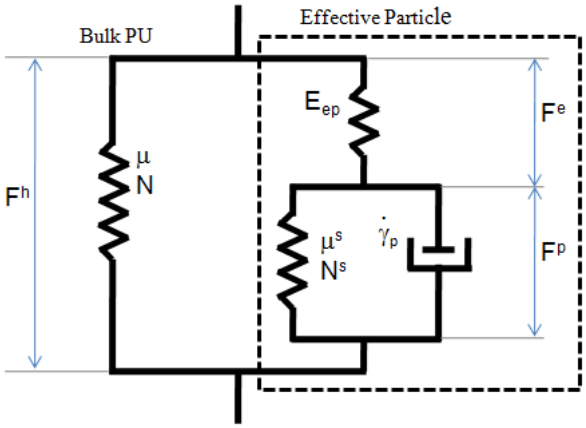

Figure 3: Mechanical analog of the proposed three-dimensional constitutive model for predicting the finite deformation response of PU-MTM nanocomposites.

$$\mathbf{F} = \mathbf{F}^h = \mathbf{F}^e\mathbf{F}^p \tag{3}$$

where $\mathbf{F}$ is the overall macroscopic deformation gradient, $\mathbf{F}^h$ is the deformation gradient acting on the hyperelastic rubbery network, i.e. bulk PU; $\mathbf{F}^e$ and $\mathbf{F}^p$ are the elastic and plastic deformation gradients acting on the effective particle. The evolution equation of the plastic deformation gradient can be determined as

$$\dot{\mathbf{F}}^p = \mathbf{D}^p\mathbf{F}^p \tag{4}$$

where $\mathbf{D}^p$ is rate of deformation following a constitutive equation prescribed later. The total Cauchy stress $\mathbf{T}$ is distributed to the bulk PU and the effective particle as

$$\mathbf{T} = \mathbf{T}^h + \mathbf{T}^{ep} \tag{5}$$

where $\mathbf{T}^h$ is the Cauchy stress acting on the bulk PU and $\mathbf{T}^{ep}$ is the Cauchy stress acting on the effective particle. $\mathbf{T}^h$ captures the resistance to entropy change in the bulk PU chains due to molecular network orientation and is modeled by the Langevin chain based eight-chain model capturing the large stretch hyperelastic behavior (Arruda and Boyce, 1993b). The eight-chain model has previously been used to model strain hardening in amorphous polymers (Arruda and Boyce, 1993a; Arruda et al., 1995). Due to the three-dimensional network aspect of the polymer chains, the model has been shown to successfully predict the large deformation stress-strain response of rubbery materials (Wang et al., 2001) as well as the strain-induced amorphous chain orientation in glassy polymers upon large deformation (Arruda et al., 1995; Boyce et al., 1994).

$\mathbf{T}^h$, taken to be deviatoric, is given as

$$\mathbf{T}^h = (1 - v_{ep})\frac{\mu}{3J}\frac{\sqrt{N}}{\lambda_{chain}}\mathcal{L}^{-1}[\frac{\lambda_{chain}}{\sqrt{N}}][\mathbf{B} - \lambda_{chain}^2\mathbf{I}] \tag{6}$$

where $(1 - v_{ep})$ is the volume fraction of bulk PU, $J = det\mathbf{F}^h$, $\mu = nk\Theta$ is the initial hardening modulus with chain density n, Boltzmann's constant k and absolute temperature Θ, N is the number of statistical rigid links between entanglements, $\mathbf{B} = \mathbf{F}^h\mathbf{F}^{hT}$ is the isochoric left Cauchy-Green tensor where $< . >^T$ denotes the transpose of $< . >$, $\lambda_{chain} = \sqrt{I_1/3}$ is the stretch on each chain in the network with $I_1 = tr(\mathbf{B})$ as the first invariant of $\mathbf{B}$. $\mathcal{L}^{-1}$ is inverse Langevin function, defined as

$$\mathcal{L}(x) = coth(x) - \frac{1}{x} \tag{7}$$

providing the functionality that as λ_{chain} approaches its locking extensibility

$\sqrt{N}$, the stress increases dramatically.

The linear-elastic element of the effective particle is constitutively governed by Hooke's law as

$$\mathbf{T}^{ep} = \frac{v_{ep}}{det\mathbf{F}^e}\mathbf{C}[ln\mathbf{V}^e] \tag{8}$$

where $\mathbf{C}$ is the fourth-order isotropic elasticity tensor and $\mathbf{V}^e$ is an elastic left stretch tensor (Boyce et al., 1988). The coefficients of $\mathbf{C}$ depend on the modulus, E_{ep} and Poisson's ratio, ν of the effective particle (Wang and Arruda, 2006).

As defined above, the effective particle is composed of modified PU chains and stiff MTM nanoparticles (in-plane modulus: 270 GPa (Manevitch and Rutledge, 2004)). Due to the presence of these MTM nanoparticles, the average strain in the modified PU chains is amplified over that of the macroscopic strain to accommodate the limited strain in the nanoparticles as suggested by Mullins and Tobin (Mullins and Tobin, 1965). We incorporate this by amplifying the first invariant of stretch as suggested by Bergström and Boyce. (Bergström and Boyce, 1999)

$$\langle I_{1s}\rangle_m = X(\langle I_{1s}\rangle - 3) + 3 \tag{9}$$

where $\langle I_{1s}\rangle_m$ is the amplified first invariant of stretch, and $\langle I_{1s}\rangle$ is the first invariant of the stretch on the related modified PU chains. X is an amplification factor dependent on the volume fraction of MTM nanoparticles. Depending on the shape and properties of the fillers, and interaction among the particles, the amplification factor takes the general polynomial form of $X = 1 + av_p + bv_p{}^2$. This second order equation has been successfully used

to predict elastic response of filled polymers. In this work, this approach has been extended to the finite strain plasticity. Here, we choose the amplification factor for the Guth model (Guth, 1945; Bergström and Boyce, 1999), i.e. $a = 0.67g_p$ and $b = 1.62{g_p}^2$, hence resulting in $X = 1 + 0.67g_p v_p + 1.62{g_p}^2{v_p}^2$, where g_p is a constant typically between 4 and 10. Stress in the hyperelastic spring, $\mathbf{T}^s$, is given as (Qi and Boyce, 2005)

$$\mathbf{T}^s = (v_p)\frac{\mu^s}{3J_s}\frac{\sqrt{N^s}}{\Lambda^s_{chain}}\mathcal{L}^{-1}[\frac{\Lambda^s_{chain}}{\sqrt{N^s}}][\mathbf{B}^s - \Lambda^{s^2}_{chain}\mathbf{I}] \tag{10}$$

where $J_s = det\mathbf{F}^p$, $\mu^s = n^s k\Theta$, $\mathbf{B}^s = \mathbf{F}^p\mathbf{F}^{pT}$ is the isochoric left Cauchy-Green tensor, $\Lambda^s_{chain} = \sqrt{X(\lambda^{s^2}_{chain} - 1) + 1}$ is the amplified chain stretch (Qi and Boyce, 2005). $\lambda^s_{chain} = \sqrt{I^s_1/3}$ is the stretch on each chain in the network with $I^s_1 = tr(\mathbf{B}^s)$. It is worth noting that the elastic strain should also be ideally amplified over that of the macroscopic strain. We, however, neglect this effect here since the elastic strains are very small.

The plastic driving stress $\mathbf{T}^p$ on the viscoplastic dashpot is determined from the tensorial difference between the total Cauchy stress on the effective particle $\mathbf{T}^{ep}$ and the convected network stress from hyperelastic spring element, $\mathbf{T}^s$.

$$\mathbf{T}^p = \mathbf{T}^{ep} - \frac{1}{J_s}\mathbf{F}^p\mathbf{T}^s\mathbf{F}^{pT} \tag{11}$$

$$\tau = \sqrt{\frac{1}{2}(\mathbf{T}^{p*}.\mathbf{T}^{p*})} \tag{12}$$

where τ is the shear stress and $\mathbf{T}^{p*}$ is the deviatoric portion of the plastic driving stress. The viscoplastic response activated once the isotropic resis-

tance to chain segment rotation is overcome, is prescribed constitutively, through the rate of plastic deformation, $\mathbf{D}^p$, defined as

$$\mathbf{D}^p = \dot{\gamma}^p \mathbf{N}^p \tag{13}$$

where $\dot{\gamma}^p$ is the equivalent plastic shear strain rate and $\mathbf{N^p}$ is a normalized tensor aligned with the deviatoric driving stress state,

$$\mathbf{N}^p = \frac{1}{\sqrt{2\tau}} \mathbf{T}^{p*} \tag{14}$$

$\dot{\gamma}^p$ is given as

$$\dot{\gamma}^p = \dot{\gamma}_0 exp[-\frac{\Delta G}{k\Theta}\{1 - (\frac{\tau}{s_0})\}] \tag{15}$$

where $\dot{\gamma}_0$ is the pre-exponential factor proportional to the attempt frequency, $s_0 = 0.077\mu/(1-\nu)$ is the athermal shear strength with μ as the elastic shear modulus and ν as the Poisson's ratio (Qi and Boyce, 2005; Arruda et al., 1993). ΔG is the zero stress level activation energy, k is the Boltzmann's constant and Θ is absolute temperature.

4. Material Parameters Identification

The summary of the constitutive model and the required material parameters are listed in Table 2. The parameters needed to be determined for the bulk PU are μ and N (c.f. Equation 6). The true stress-strain constitutive response for PU was utilized in order to determine these parameters (c.f. Figure 1). The inverse Langevin function, $\mathcal{L}^{-1}(x)$, is evaluated by a Padé approximation given as:

Material	Constitutive elements	Parameters	Constitutive equation
Bulk PU	Hyperelastic rubbery spring element	μ, N	$\mathbf{T}^h = (1 - v_{ep})\frac{\mu}{3J}\frac{\sqrt{N}}{\lambda_{chain}}\mathcal{L}^{-1}[\frac{\lambda_{chain}}{\sqrt{N}}][\mathbf{B} - \lambda_{chain}^2\mathbf{I}]$
Effective Particle	Linear elastic spring element	E_{ep}, ν	$\mathbf{T}^{ep} = \frac{v_{ep}}{det\mathbf{F}^e}\mathbf{C}[ln\mathbf{V}^e]$
	Hyperelastic rubbery spring element	μ^s, N^s	$\mathbf{T}^s = (v_p)\frac{\mu^s}{3J_s}\frac{\sqrt{N^s}}{\Lambda^s_{chain}}\mathcal{L}^{-1}[\frac{\Lambda^s_{chain}}{\sqrt{N^s}}][\mathbf{B}^s - \Lambda^{s^2}_{chain}\mathbf{I}]$ $X = 1 + 0.67g_p v_p + 1.62{g_p}^2{v_p}^2$
	Viscoplastic dashpot element	$\dot{\gamma}_0, \Delta G$	$\dot{\gamma}^p = \dot{\gamma}_0 exp[-\frac{\Delta G}{k\Theta}\{1 - (\frac{\tau}{s_0})\}]$

Table 2: Summary of constitutive model and material parameters

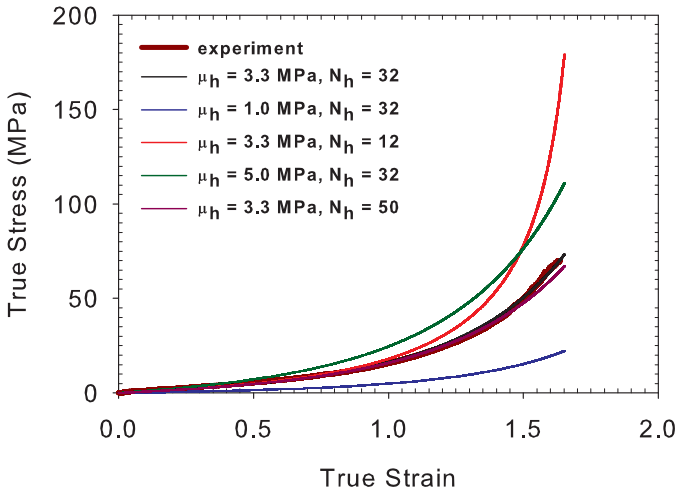

Figure 4: Material parameter identification and parametric study for the non-linear elastic spring for the bulk PU.

$$\mathcal{L}^{-1}(x) = \frac{x(3-x^2)}{1-x^2} \tag{16}$$

We determine $\mu = 3.3$ MPa and $N = 32.0$. The locking stretch, hence, is $\sqrt{N} = 5.66$ (Wang and Arruda, 2006). Figure 4 shows the curve fitting using the estimated parameters. A parametric study of μ and N is also shown.

The material parameters needed to be determined for the effective particle are E_{ep}, t, ν, μ^s, N^s, $\dot{\gamma}_0$, ΔG and g_p (c.f. Equations 2, 8, 10 and 15). The Young's modulus of the PU-MTM nanocomposite, E_c, is the contribution from that of bulk PU, E_b, and effective particle, E_{ep}. E_b and E_c for bulk PU and the entire series of PU-MTM nanocomposites respectively were determined experimentally (initial slope of true stress-strain curves, c.f. Table 1). v_{ep} and E_{ep} were then determined from the traditional Voigt upper

bound (Voigt, 1889) for a linear elastic isotropic material as:

$$v_{ep} = \frac{E_c - E_b}{E_{ep} - E_b} \tag{17}$$

E_{ep} can be determined from the above equation using the value of E_c for PU-MTM20 nanocomposite. At v_p= 0.20; $v_{ep} = 1$ suggesting $E_{ep} = 3.6$ GPa. The values of t (for each nanocomposite) were determined from Equation 2 as:

$$t = \frac{t_b(v_{ep} - v_p)}{2} \tag{18}$$

In reality, the interphase thickness is constant over the entire nanocomposites series (Kaushik et al., 2009) and the variation of t here is a result of the approximated elasticity formulation and model geometry simplification. The focus of the current work lies in predicting the finite deformation response of multi-layered nanocomposites. Nevertheless, more accurate approaches to elasticity capturing the stiffness changes with MTM nanoparticles have recently been investigated for these nanocomposites (Li et al., 2010a,b). The Poisson's ratio, ν, was assumed to be 0.48. This is a reasonable assumption as PU is rubbery at room temperature (glass transition temperature, $T_g \sim -76\,^{\circ}$C (Kaushik et al., 2009)). Additionally, changes in ν do not affect the results strongly. The material constants $\dot{\gamma}_0$ and ΔG were obtained by rewriting Equation 15 as

$$\tau = cln\dot{\gamma}^p + b, \tag{19}$$

where $c = \frac{s_0}{D}$, $b = \frac{s_0}{D}(D - ln\dot{\gamma}_0)$, and $D = \frac{\Delta G}{k\Theta}$. These constants were determined experimentally from true stress-strain curves at two different strain

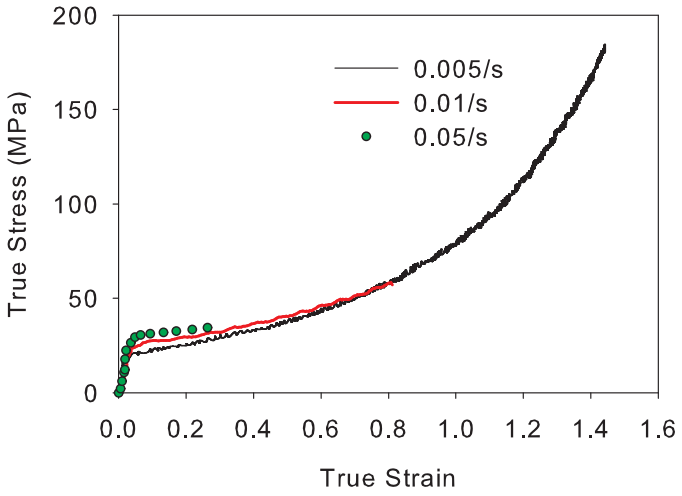

Figure 5: True stress-strain constitutive response of PU-MTM nanocomposites with 5 v.% MTM nanoparticles at $\dot{\epsilon} = 0.005/\text{s}$, $= 0.01/\text{s}$ and $0.05/\text{s}$.

rates in uniaxial tension. We choose the PU-MTM5 nanocomposite to determine these parameters (Figure 5). The nanocomposite demonstrates a dependence of yield strength on strain rate. The yield strength increased with an increase in the strain rate. The equivalent shear stress, τ and shear strain, γ^p are related to the uniaxial stress, σ and uniaxial strain, ϵ respectively by

$$\tau = \frac{\sigma}{\sqrt{3}}, \tag{20}$$

and

$$\gamma^p = \sqrt{3}\epsilon \tag{21}$$

Bulk PU		Effective	Particle					
μ (MPa)	N	t (nm)	E_{ep} (GPa)	ν	$\dot{\gamma}_0$ $(10^{49}s^{-1})$	ΔG $(10^{-19}J)$	μ^s (MPa)	N^s
3.3	32.0	1.83(5)	3.6	0.48	1.01	5.25	4.8	10.0
		2.04(7)						
		2.24(10)						
		2.84(12)						
		4.60(20)						

Table 3: Material parameters for bulk PU and effective particle. The numbers in parenthesis represent the volume fraction of MTM nanoparticles.

The material parameters g_p, μ^s and N^s were determined by fitting the strain hardening portion of the true stress-strain response curve for the PU-MTM5 nanocomposite. We obtained $g_p = 10$, $\mu^s = 3.6$ MPa and $N^s = 12.0$.

5. Modeling Results and Discussion

The three-dimensional constitutive model for PU and PU-MTM nanocomposites at finite deformations was implemented into MATLAB® (The Math Works Inc., Natick, MA) for uniaxial tension simulations. The material parameters for the bulk PU and the PU-MTM nanocomposites are listed in Table 3.

Figure 6 shows the modeling and experimental results for uniaxial tension tests at $\dot{\epsilon} = 0.005$/s. The model results are in excellent agreement with the

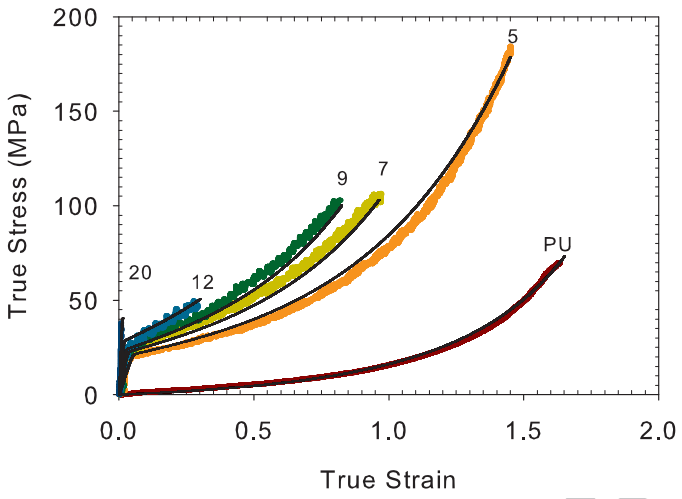

Figure 6: Model results (in black) and experimental results (in color) for the finite deformation constitutive response of PU and PU-MTM nanocomposites at $\dot{\epsilon} = 0.005/s$.

experimental results and demonstrate the ability of the constitutive model to accurately predict the constitutive response of PU-MTM nanocomposites across a wide range of volume fraction of MTM nanoparticles. It is important to note here that only the bulk PU and the PU-MTM5 nanocomposite response curves were fitted and used to determine the material parameters; the rest of the responses have been predicted with the same set of parameters. Clearly, the model captures the major characteristic features of PU-MTM nanocomposites response to large strain uniaxial deformation including the initial linear elastic response, volume fraction dependent yield strength and post-yield strain hardening.

It is important to note that the application of amplified stretch was a significant reason for the success of the constitutive model to accurately pre-

dict the post-yield constitutive response of PU-MTM nanocomposites. Figure 7 shows the model results without the amplified stretch. Here, again the PU-MTM5 nanocomposite was used to determine μ^s and N^s. We found $\mu^s = 5.3\ MPa$ and $N^s = 4.5$. Clearly, the constitutive model without amplified stretch, although able to predict the initial elastic response and yield strength, is not able to predict the post-yield strain hardening response. This suggests that the mechanism of amplified stretch is vital in predicting the constitutive response of layered PU-MTM nanocomposites.

The presence of strain-rate dependent viscoplastic dashpot allows the prediction of the strain-rate dependent constitutive response of PU-MTM nanocomposites. Figure 8 shows the model predictions for finite deformation response of PU-MTM5 at $\dot{\epsilon} = 0.01$/s and 0.05/s. The model captures the strain-rate dependent yield strength and post-yield strain hardening response fairly well.

We believe that proposed model may be capable of predicting the finite deformation response of these multi-layered nanocomposites in various other deformation states, e.g. uniaxial compression, plane strain compression/tension tests. It is being acknowledged here that to this date the model has only been validated in the in-plane direction i.e. in uniaxial tension because of the nature of the nanocomposite films. These nanocomposite films generally are thin materials with very small thicknesses. Loading these materials in the out-of-plane direction is virtually not possible and may not be that significant.

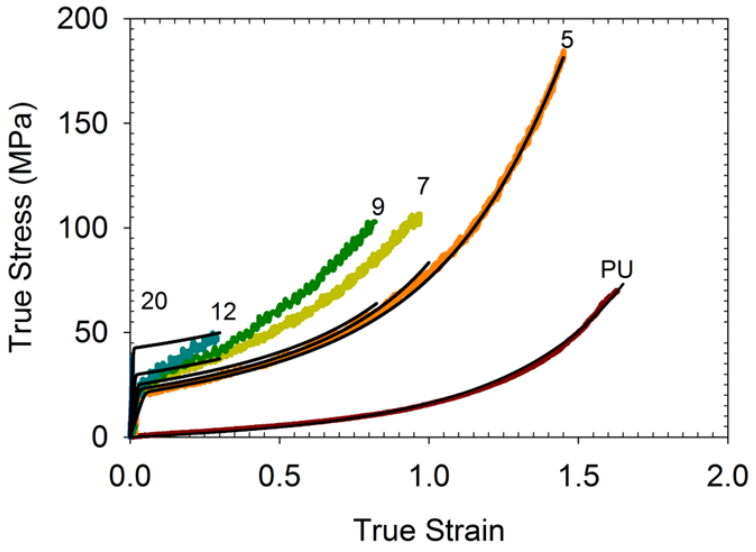

Figure 7: Model results (in black) and experimental results (in color) for the finite deformation constitutive response of PU and PU-MTM nanocomposites. The model results are without any amplified stretch, i.e. $X = 1$.

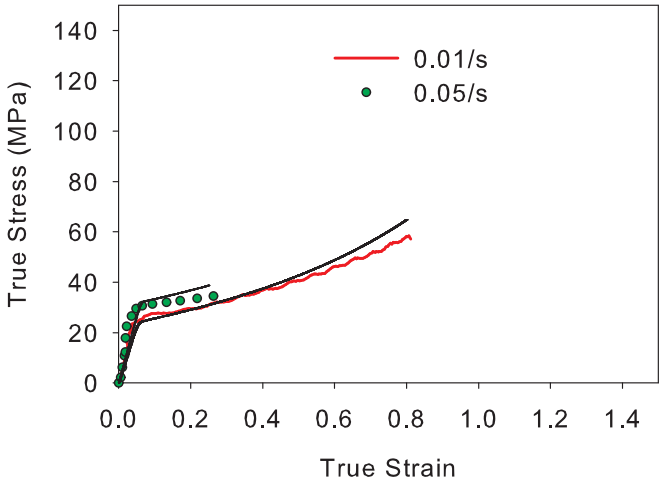

Figure 8: Model predictions (in black) and experimental results (in color) for the finite deformation constitutive response of PU-MTM5 at $\dot{\epsilon} = 0.01/\text{s}$ and $0.05/\text{s}$.

6. Summary and Conclusions

This paper presented several important aspects in the finite deformation response of multi-layered PU-MTM nanocomposites:

- The interphase region plays a vital role in the finite deformation response of the nanocomposites owing to large surface area to volume ratio. The effect of interphase is studied via an effective particle that consisted of stratified layers of MTM nanoparticles and the interphase region comprising modified PU matrix.

- The presence of MTM nanoparticles leads to large strain-gradients during the finite deformation of nanocomposites resulting in an increased strain-hardening response. The current constitutive model with the aid

of amplified stretch accounts for the increase in these strain gradients increased with volume fraction of MTM nanoparticles. The stretch amplified as a function of the volume fraction of MTM nanoparticles was a significant reason for the success of the constitutive model to accurately predict the post-yield response of the PU-MTM nanocomposites.

- In the present work, the finite deformation response of nanocomposites is examined only in uniaxial tension deformation state, only at a room temperature and at a limited strain-rate range but the current constitutive model may be used to predict temperature and strain-rate effects over broad ranges. Further experimental tests are needed to verify the efficacy of the constitutive model at high strain rates and/or where temperature effects play a role.

7. Acknowledgements

This research was supported by the Office of Naval Research through grant $00014-06-1-0473$.

8. References

Adnan, A., Sun, C., Mahfuz, H., 2007. A molecular dynamics simulation study to investigate the effect of filler size on elastic properties of polymer nanocomposites. Comp. Sci. Tech. 67 (3-4), 348–356.

Anthoulis, G., Kontou, E., 2008. Micromechanical behaviour of particulate polymer nanocomposites. Polymer 49 (7), 1934–1942.

Arruda, E., Boyce, M., 1993a. Evolution of plastic anisotropy in amorphous polymers during finite straining. Int. J. Plast. 9 (6), 697–720.

Arruda, E., Boyce, M., 1993b. A three-dimensional constitutive model for the large stretch behavior of elastomers. J. Mech. Phy. Solids 41 (2), 389–412.

Arruda, E., Boyce, M., Jayachandran, R., 1995. Effects of strain-rate, temperature and thermomechanical coupling on the finite strain deformation of glassy-polymers. Mech. Mater. 19 (2-3), 193–212.

Arruda, E., Boyce, M., Quintus-Bosz, H., 1993. Effects of initial anisotropy on the finite strain deformation behavior of glassy polymers. Int. J. Plast. 9 (7), 783–811.

Bergström, J., Boyce, M., 1999. Mechanical behavior of particle filled elastomers. Rubber Chem. Technol. 72 (4), 633–656.

Boutaleb, S., Zaïri, F., Mesbah, A., Naït-Abdelaziz, M., Gloaguen, J., Boukharouba, T., Lefebvre, J., 2009. Micromechanics-based modelling of stiffness and yield stress for silica/polymer nanocomposites. Int. J. Solids Struct. 46 (7-8), 1716–1726.

Boyce, M., Arruda, E., Jayachandran, R., 1994. The large-strain compression, tension, and simple shear of polycarbonate. Polym. Eng. Sci. 34 (9), 716–725.

Boyce, M., Parks, D., Argon, A., 1988. Large inelastic deformation of glassy polymers. part i: rate dependent constitutive model. Mech. Mater. 7 (1), 15–33.

Brune, D., Bicerano, J., 2002. Micromechanics of nanocomposites: comparison of tensile and compressive elastic moduli, and prediction of effects of incomplete exfoliation and imperfect alignment on modulus. Polymer 43 (2), 369–387.

Budiansky, B., 1965. On the elastic moduli of some heterogeneous materials. J. Mech. Phys. Solids 13 (4), 223–227.

Budiansky, B., Wu, T., 1962. Theoretical prediction of plastic strains of polycrystals. Proc. 4th US Nat. Cong. Appl. Mech. 35, 1175–1185.

Decher, G., 1997. Fuzzy nanoassemblies toward layered polymeric multicomposites. Science 277 (5330), 1232–1237.

Einstein, A., 1906. A new determination of molecular dimensions. Ann. Phys. 19 (2), 289–306.

Fisher, F., Bradshaw, R., Brinson, L., 2003. Fiber waviness in nanotube-reinforced polymer composites—I: modulus predictions using effective nanotube properties. Compos. Sci. Tech. 63 (11), 1689–1703.

Govindjee, S., 1997. An evaluation of strain amplification concepts via Monte Carlo simulations of an ideal composite. Rubber Chem. Tech. 70, 25–37.

Guth, E., 1945. Theory of filler reinforcement. J. Appl. Phy. 16, 20–25.

Halpin, J., 1969. Stiffness and expansion estimates for oriented short fiber composites. J. Compos. Mater. 3 (4), 732–734.

Kaushik, A., 2010. Deformation mechanisms in polymer-clay nanocomposites. Ph.D. Thesis, The University of Michigan, Ann Arbor.

Kaushik, A., Podsiadlo, P., Qin, M., Shaw, C., Waas, A., Kotov, N., Arruda, E., 2009. The role of nanoparticle layer separation in the finite deformation response of layered polyurethane-clay nanocomposites. Macromolecules 42 (17), 6588–6595.

Ke, Y., Stroeve, P., 2010. Preparation and properties of polyurethane dispersions with aromatic/aliphatic mixed diisocyanate. Manuscript in Preparation.

Kotov, N., 2001. Ordered layered assemblies of nanoparticles. Mater. Res. Bull. 26 (12), 992–997.

Larkin, L., Calve, S., Kostrominova, T., Arruda, E., 2006. Structure and functional evaluation of tendonskeletal muscle constructs engineered in vitro. Tissue Eng. 12 (11), 3149–3158.

Li, Y., Waas, A., Arruda, E., 2010a. A closed-form, hierarchical, multi-interphase model for composites—derivation, verification and application to nanocomposites. J. Mech. Phy. Solids, in press.

Li, Y., Waas, A., Arruda, E., 2010b. The effect of the interphase and strain gradients on the elasticity of lbl polymer/clay nanocomposites. Manuscript in review.

Luo, J., Daniel, I., 2003. Characterization and modeling of mechanical behavior of polymer/clay nanocomposites. Comp. Sci. Tech. 63 (11), 1607–1616.

Manevitch, O. L., Rutledge, G. C., 2004. Elastic properties of a single lamella of montmorillonite by molecular dynamics simulation. J. Phy. Chem. 108 (4), 1428–1435.

Mooney, M., 1951. The viscosity of a concentrated suspension of spherical particles. J. Colloid Sci. 6 (2), 162–170.

Mori, T., Tanaka, K., 1973. Average stress in matrix and average elastic energy of materials with misfitting inclusions. Acta Met. 21 (5), 571–574.

Mullins, L., Tobin, N., 1965. Stress softening of rubber vulcanizates. part I. use of strain amplification factor to describe the elastic behavior of filler-reinforced vulcanized rubber. J. Appl. Poly. Sci. 9 (9), 2993–3009.

Odegard, G., Clancy, T., Gates, T., 2005. Modeling of the mechanical properties of nanoparticle/polymer composites. Polymer 46 (2), 553–562.

Podsiadlo, P., Kaushik, A., Arruda, E., Waas, A., Shim, B., Xu, J., Nandivada, H., Pumplin, B., Lahann, J., Ramamoorthy, A., Kotov, N., 2007. Ultrastrong and stiff layered polymer nanocomposites. Science 318, 80–83.

Qi, H., Boyce, M., 2005. Stress-strain behavior of thermoplastic polyurethanes. Mech. Mater. 37 (8), 817–839.

Ramanathan, T., Liu, H., Brinson, L., 2005. Functionalized swnt/polymer nanocomposites for dramatic property improvement. J. Polym. Sci., Part B: Polym. Phys. 43 (17), 2269–2279.

Sheng, N., Boyce, M., Parks, D., Rutledge, G., Abes, J., Cohen, R., 2004. Multiscale micromechanical modeling of polymer/clay nanocomposites and the effective clay particle. Polymer 45 (2), 487–506.

Smallwood, H. M., 1944. Limiting law of the reinforcement of rubber. J. Appl. Phy. 15, 758–766.

Smith, J., Bedrov, D., Smith, G., 2003. A molecular dynamics simulation study of nanoparticle interactions in a model polymer-nanoparticle composite. Comp. Sci. Tech. 63 (11), 1599–1605.

Vaia, R., Sauer, B., Tse, O., Giannelis, E., 1997. Relaxations of confined chains in polymer nanocomposites: Glass transition properties of poly(ethylene oxide) intercalated in montmorillonite. J. Polym. Sci.: Part B: Polym. Phys. 35 (1), 59–67.

Vand, V., 1996. Viscosity of solutions and suspensions. I. theory. J. Phys. Chem. 52 (2), 277–299.

Voigt, W., 1889. The relation between the two elastic moduli of isotropic materials. Ann. Phys. 38, 573–587.

Wang, Y., Arruda, E., 2006. Constitutive modeling of a thermoplastic olefin over a broad range of strain rates. J. Eng. Mater. Technol. 128 (4), 551–558.

Wang, Y., Arruda, E., Przybylo, P., 2001. Characterization and constitutive modeling of a plasticized poly(vinyl chloride) for a broad range of strain rates. Rubber Chem. Tech. 74 (4), 560–573.

Zaïri, F., Naït-Abdelaziz, M., Gloaguen, J., Lefebvre, J., 2010a. A physically-based constitutive model for anisotropic damage in rubber-toughened glassy polymers during finite deformation, in press. Int. J. of Plast.

Zaïri, F., Naït-Abdelaziz, M., Gloaguen, J., Lefebvre, J., 2010b. Constitutive modelling of the large inelastic deformation behaviour of rubber-toughened poly (methyl methacrylate): effects of strain rate, temperature and rubber-phase volume fraction. Model. Sim. Mat. Sci. and Eng. 18, 1–22.